

## Count rate studies for the Micro-Vertex-Detector

Marius C. Mertens <sup>1</sup>, Thomas Würschig <sup>2</sup>  
René Jäkel <sup>3</sup>

<sup>1</sup> Forschungszentrum Jülich GmbH, Institut für Kernphysik I  
D-52455 Jülich, Germany  
Email: m.mertens@fz-juelich.de

<sup>2</sup> Rheinische Friedrich-Wilhelms-Universität Bonn, Helmholtz-Institut für  
Strahlen- und Kernphysik  
Nussallee 14-16, D-53115, Bonn, Germany  
Email: t.wuerschig@hiskp.uni-bonn.de

<sup>3</sup> Technische Universität Dresden, Institute for Nuclear and Particle Physics  
Zellescher Weg 19, D-01062 Dresden, Germany

01/04/2010  
(Modified version)

## **Abstract**

An important input parameter for the design of tracking detectors is the expected hit rate the detector has to handle. This hit rate determines the required operation speed, the maximum dead time and the data rate for the detector. Moreover, the maximum count rate on single channels together with the integrated and averaged count rate to be expected for individual frontends deliver fundamental input for the ASIC development of the frontend electronics and allow to fix basic parameters needed for specification.

This note presents the results of two different count rate studies which have been carried out consecutively for the MVD. The results allow a comparison as they have been carried out independently and apply different methods. The second study includes updated information concerning the MVD layout in addition. The purpose of both studies is to assess the consequences of the expected occupancy and to estimate an upper limit for the maximum hit rates occurring on single channels and frontends.

# 1 Introduction

The hit occupancy within the MVD plays an important role for detector development since it defines the required link speed and the maximum rates to be handled by frontend electronics. Both are connected to material budget and power dissipation of the detector. The hit rates obtained on single detector elements translate into the generated data output of the specific frontends connected.

The acquired data is directly associated with the particle tracks which penetrate the detector volume. Hence, the general particle track distribution created in beam-target reactions deliver first results for both the occupancy and the momentum range of particles in different detector regions. With this input, count rates on single channels, frontends and detector parts can be extracted by applying a dedicated model which includes a digitization of the tracks.

The main scope of this detector note is to summarize all count rate studies done so far. Even though there are still some uncertainties and simplifications, they allow more profound estimates of the expected hit rates within the MVD and the overall data load of the whole detector. Current specifications given for frontend electronics and data generation refer to results of the presented studies [1]. Of course, all numbers will be surveyed and cross-checked in case of significant modification either in the software, the detector model or any other specification (e.g. the expected interaction rate) which potentially have an impact on the obtained results.

## 2 Count rate studies (1)

### 2.1 General description

The count rate studies summarized in this chapter focus on two main topics:

- The spatial distribution and the momentum range of all particles created at the primary interaction vertex.
- The extraction of count rates on individual frontends and single channels applying a detailed model for the sensor arrangement within the MVD volume.

The spatial distribution of particles emitted into different solid angles allows a mapping of the track densities and, furthermore, the calculation of the occupancy in different detector parts of the MVD. The implemented detector model is based on three different sensor types. The applied readout structures include different pixel cell sizes and a variation of the strip pitch which is adapted to both the assumed sensor size and the number of frontend chips intended to be used for readout. Even though the chosen detector model is simplified and does not include all actual modifications of the overall MVD design, the extracted numbers still allow a reasonable estimate on expected count rates and the data load to be handled by the readout electronics.

### 2.2 Input parameters

The studies were carried out for different initial reactions: antiproton-proton reactions and collisions of antiprotons with heavier nuclear targets, namely with copper and gold. The simulations were performed for different beam momenta up to

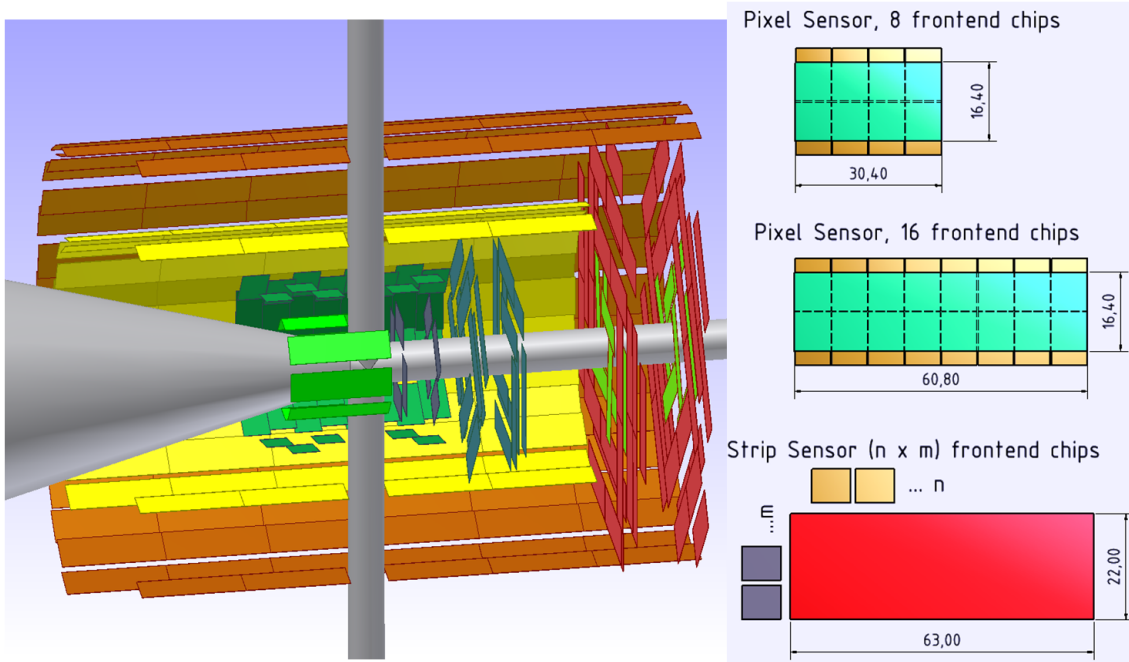


**Figure 1:** Computer aided drawing of the applied detector model (left). The pixel layers are shown in green. The strip barrel layers are highlighted in orange and yellow while the strip disk part has a red color. Right: Implemented sensor sizes together with frontend chips assumed for readout (details in text).

15 GeV/c. The particles for antiproton-proton reactions were generated with the DPM model which does not include the Coulomb part but only the hadronic part of the elastic scattering [2],[3]. For the reactions of antiprotons with copper and gold atoms the UrQMD model was used [4],[5]. In all configurations one million antiproton collisions were simulated. The studies were performed within the old PANDA framework, which is based in parts on the simulation framework developed by the BaBar collaboration [7].

The used geometry model implements two pixel barrel layers, two strip barrel layers and six pixel disk layers where the last two layers are surrounded by strip disks at outer radii. A sketch of the model can be seen in figure 1. It is consistent with the model used in [6]. The strip layers are formed by identical sensors while for the pixel part two different sensor sizes are introduced. A module consists of a sensor together with the frontend chips needed for its readout. While the sensor dimensions remained unchanged within all studies, the size of the readout structure, namely the pixel cell dimensions and the strip pitch, were varied.

Two different cell dimensions were chosen for the pixel sensors: a rectangular shape ( $50 \times 400 \mu\text{m}^2$ ) and a quadratic one ( $100 \times 100 \mu\text{m}^2$ ). The number of frontend chips was fixed to eight and sixteen for the smaller and the larger module, respectively. Hence, the number of pixel cells which are read out by one frontend double from 2880 in case of rectangular cells to 5760 for quadratic ones. For the strip frontend 128 readout channels were assumed. The strip pitch was chosen in a way that the total number of channels equals to an integer multiple of 128 at both sides.

As input for the studies the digitized detector output for both pixel and strip detectors was modeled according to the geometrical distribution of the collected charge. The hits within a module were translated into a list of contributing pixel cells or

single strip channels according to the particle trajectory through the sensor. An interaction rate of  $2 \cdot 10^7 \text{ s}^{-1}$  for antiproton-proton collision and was assumed in order to convert the total number of tracks into a corresponding count rate on single readout channels. Referring to reference [14] the interaction rate set for copper and gold is reduced by a factor of 50 and 100, respectively. The count rate of an individual frontend results from the sum over all appropriate channels.

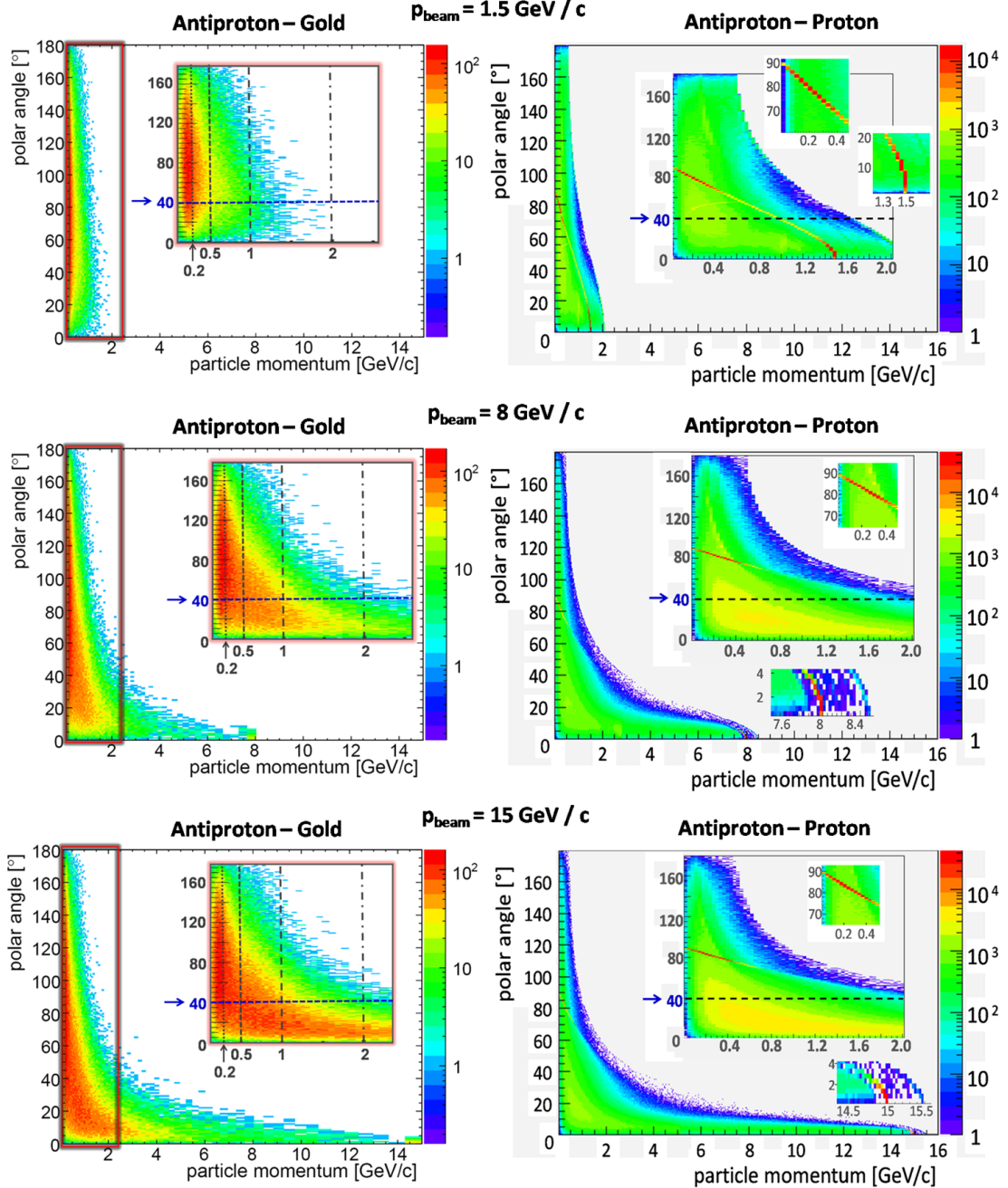


**Figure 2:** Track densities for three different beam momenta and two reaction channels plotted colour-coded against particle momentum and solid angle. The low momentum range below 2 GeV/c is enlarged in the inlay for all cases. The dashed line at  $\theta = 40^\circ$  indicates the crossover from the MVD barrel part to the MVD disk part. The two elastic peaks visible in antiproton-proton collisions are expanded additionally.

## 2.3 Results

### 2.3.1 Particle track distributions

Besides the spatial distribution, the corresponding kinetic energy of all particles emitted from the primary interaction vertex delivers an important input for the MVD detector development. Therefore, the particle momentum and the polar angle are plotted in a 2D histogram. Results for antiproton-proton and antiproton-gold collisions at three different beam momenta are shown in figure 2.

Since PANDA is a fixed target experiment the particles have an additional boost in the laboratory frame. This is reflected by a high track density in forward direction. Particle momenta range from values around 100 MeV/c up to the initial beam momentum. Hence, two orders of magnitude are spanned at maximum beam momentum. For antiproton-proton collisions some light particles (mostly pions) can exceed the beam momentum by up to 500 MeV/c.

High momentum particles are focused to forward directions at polar angles smaller than  $40^\circ$ . This region is covered by the MVD disk layers. Particles emitted at higher polar angles up to  $160^\circ$  are crossing the barrel part. There, a band of low-energetic particles is populated. In the backward region ( $\theta > 90^\circ$ ) particle momenta stay below 1 GeV/c. With higher beam momenta the band widens to roughly 2 GeV/c in the intermediate region going from  $\theta = 90^\circ$  to  $\theta = 40^\circ$ .

In case of antiproton-gold reactions particles with a momentum around 200 MeV/c are most prominent. They are distributed nearly isotropic. For higher beam momenta particles within an enlarged momentum range at the intermediate region and high energetic particles in forward direction are additionally created with the same occurrence. The situation is different for antiproton-proton collisions. Here, the emission of lower energetic particles with momenta below 1 GeV/c to forward directions is favoured. Moreover, the highest track density is represented by the two elastic peaks of low energetic particles around  $\theta = 90^\circ$  and high energetic particles at very small polar angles. This result indicates a significant contribution of elastic scattering processes within antiproton-proton reactions.

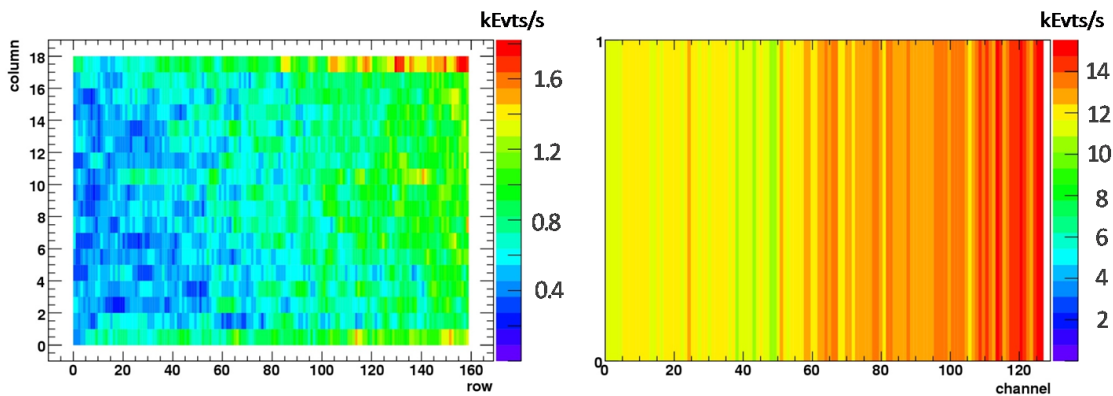


**Figure 3:** Distribution of the count rates for pixel cells (left) and long strips (right) within the frontend of highest occupancy. The highest rates occurring on single strip channels are exceeding those of the single pixel cells by nearly one order of magnitude. The results are obtained for rectangular pixel cells and a strip pitch of 50  $\mu\text{m}$  in one million antiproton-proton collisions at 6 GeV/c.

### 2.3.2 Count rates

The count rates for individual frontends and single channels can be extracted based on the track distribution discussed in the previous chapter. The integrated track density on the pixel modules is certainly larger compared to the nearly equally sized strip modules, since they are situated closer to the primary interaction point and the beam pipe. Hence, the pixel modules cover a bigger solid angle and smaller polar angles, respectively. On the other hand, the effective area to be read out by one single strip channel is much bigger than that for a single pixel cell. Therefore, the maximum count rates on single channels are caused by the long strips. They exceed the values for single pixel cells by nearly one order of magnitude (see figure 3).

The integrated count rate on single pixel frontends is slightly lower than for frontends reading out the long strips. However, both are in the same order of magnitude. The count rates on single strip channels and frontends along the short sensor side is reduced by roughly a factor of two. A summary of the maximum count rates for different setups is given in table 1. Changing from antiproton-proton collisions to reactions with heavier nuclear targets the overall tendency is an decrease in the count rates by one order of magnitude.

The count rates in different detector regions again reflect the track density distribution described in the previous chapter. As an example, the maximum rate appearing on frontend level is plotted in figure 4 for all individual modules of the detector lay-

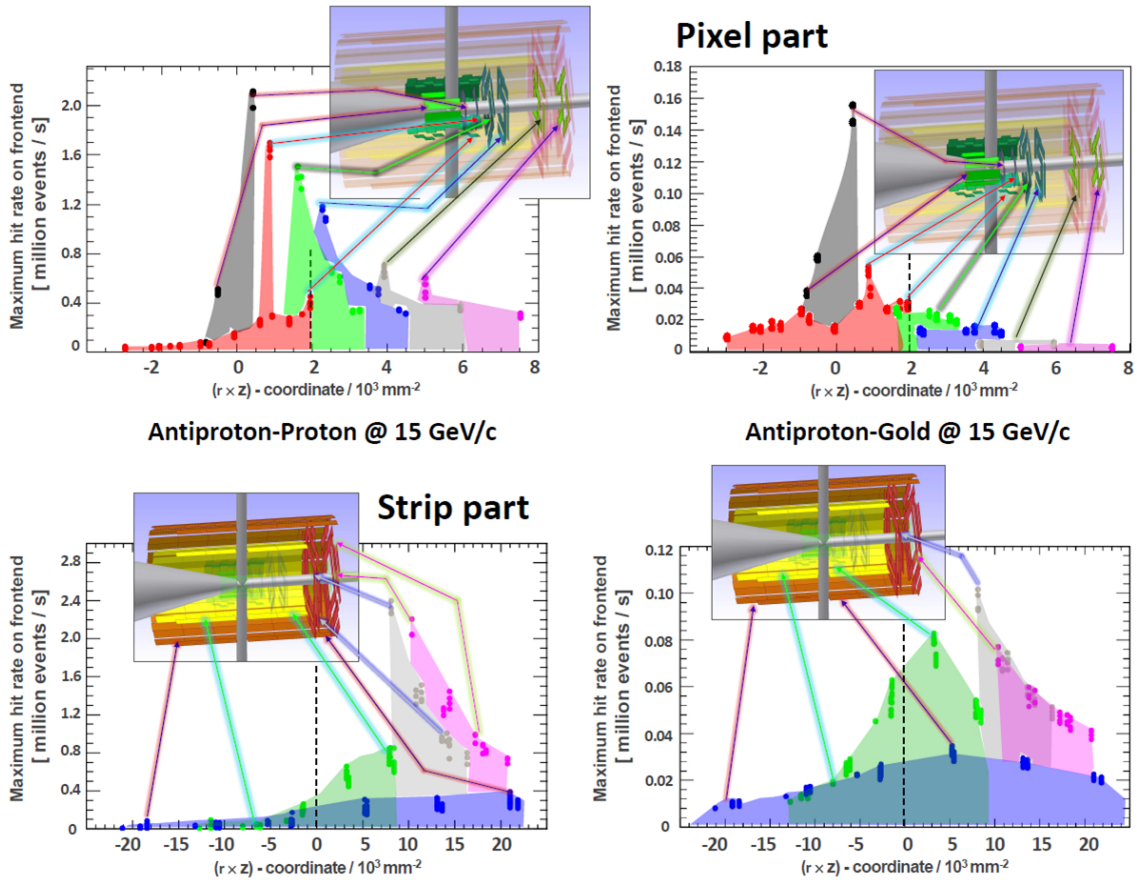


**Figure 4:** Maximum count rates on frontend level appearing at modules within different detector layers. Results obtained for quadratic pixel cell size and a pitch of 100  $\mu\text{m}$ .

<b>Pixel part</b>			
Target (Generator)	Beam momentum / [GeV/c]	Pixel size / [ $\mu\text{m}^2$ ]	Maximum count rate on frontend / [Mevts/s]
proton (DPM)	6	100 × 100	1.46
proton (DPM)	6	50 × 400	2.10
proton (DPM)	15	100 × 100	1.64
proton (DPM)	15	50 × 400	2.48
Cu (UrQMD)	4	100 × 100	0.055
Cu (UrQMD)	4	50 × 400	0.080
Au (UrQMD)	15	100 × 100	0.156
Au (UrQMD)	15	50 × 400	0.202
<b>Strip part</b>			
Target (Generator)	Beam momentum / [GeV/c]	Pitch long / short side / [ $\mu\text{m}$ ]	Maximum count rate on frontend long / short side / [Mevts/s]
proton (DPM)	6	54 / 57	1.56 / 0.62
proton (DPM)	6	98 / 86	1.86 / 0.78
proton (DPM)	6	164 / 171	2.72 / 1.40
proton (DPM)	15	54 / 57	2.00 / 0.80
proton (DPM)	15	98 / 86	2.44 / 0.94
proton (DPM)	15	164 / 171	3.38 / 1.78
Cu (UrQMD)	4	54 / 57	0.036 / 0.020
Cu (UrQMD)	4	98 / 86	0.047 / 0.029
Cu (UrQMD)	4	164 / 171	0.071 / 0.040
Au (UrQMD)	15	54 / 57	0.082 / 0.045
Au (UrQMD)	15	98 / 86	0.102 / 0.056
Au (UrQMD)	15	164 / 171	0.152 / 0.086

**Table 1:** Maximum count rates in units of million events per second (Mevts/s) appearing in different setups on pixel and strip frontends. In all cases 1 million collisions were simulated. Even though the pixel modules cover a bigger solid angle at regions with the highest track densities of the MVD, both values are in the same order of magnitude due to the larger area to be read out by single strips compared to the pixel cells (see also figure 3). The higher count rates of single channels is counter-balanced by the reduced number of channels per frontend.

ers. Since the radius of a module is not good to distinguish different modules in the same barrel layer and the  $z$ -coordinate is not a good measure for modules located in the disk layers, the product of radius and  $z$ -position was chosen to separate modules from the same layer. For both pixel and disk part the highest rates appear in the innermost disk layer within antiproton-proton collisions at maximum beam momentum. The peak values are reaching 2.5 Mevts/s and 3.4 Mevts/s for the pixel and the strip part, respectively. Moreover, the count rate in the barrel layers is also peaking in the forward part. Changing from antiproton-proton collisions to antiproton-gold reactions, this effect is increased. The maximum count rate in the innermost barrel layers is nearly as big as the highest values obtained in the innermost disk layers.

### 3 Count Rate Studies (2)

This study focuses on the analysis of the data rate generated by the MVD. In order to assess the expected data load, antiproton-proton interactions have been simulated with the DPM [2],[3] event generator. The particles were tracked through the detector using *Geant 3* [8] as well as *Geant 4* [9],[10] for selected values and digitized within the PandaROOT framework (revision 4500) [11]. Besides the investigations for the central MVD, two additional forward strip disks were introduced. The main objective of this work was to evaluate the data rates in this region in order to study the feasibility of using double sided strip sensors as implemented in the outer strip disks of the central MVD.

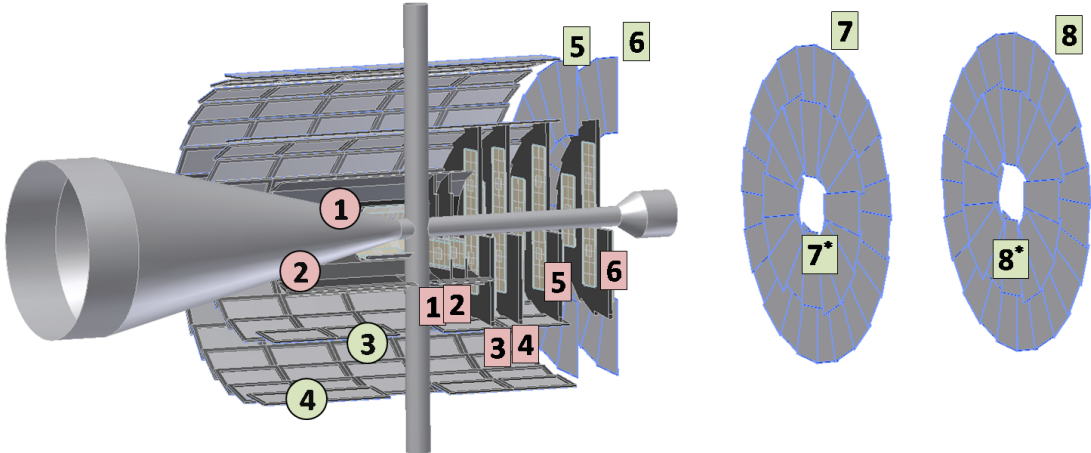


**Figure 5:** Detector Geometry: The barrel layers are numbered from the inside to the outside. The two innermost barrel layers consist of pixel detectors, the two outer layers consist of strip detectors. The disks are numbered from upstream to downstream (left to right) where the first two small disks are pixel disks. Next to these are four large disks, the first two comprising pixel detectors only, while the third and fourth large disk have an additional strip detector part in the outer region. The additional two disks farthest downstream consist of an outer ring of strip detectors identical to the standard large MVD disks while their inner ring consists of the same trapezoidal strip sensors, but shifted towards the inside.

Generator	Propagator	Beam Momentum / GeV/c	Event Count
DPM	Geant 3	2..15, Step size: 1 GeV/c	100000
DPM	Geant 4	2, 4, 7, 10, 13, 15	50000

**Table 2:** Selected input parameters for the simulation

### 3.1 Detector Geometry

For the simulations, the beam and target pipes as well as the MVD geometry version *MVD-1.0\_Pv-1.0\_Sv-1.0* [12] with two additional forward disks at  $z = 40$  cm and  $z = 60$  cm were taken into account as components (see Fig. 5).

The additional forward disks consist of an inner and an outer disk of trapezoidal strip modules. While the outer disk is identical to that of the regular MVD strip disks, the inner disk is comprised of the same trapezoidal strip modules but shifted inwards. This procedure results in relatively large overlap regions for the additional inner strip disk, leading to an overestimate of the generated data for this detector part. However, for the sole purpose of introducing sensitive material into the interesting region downstream of the MVD, this rather crude procedure suffices.

### 3.2 Simulation Parameters

The data simulated for this analysis consists of samples for different beam momenta from 2 GeV/c up to 15 GeV/c with 100000 events per beam momentum. For the rate study, the DPM generator has been chosen as event source and the tracking was performed using *Geant 3*. For comparison, a second dataset of DPM data with *Geant 4* as propagator has been analyzed, but due to the lower speed only for selected beam momenta and 50000 events each (see table 2).

The implemented digitization was done with a quadratic pixel cell size with a side length of 100  $\mu\text{m}$  and a pitch of 120  $\mu\text{m}$  and 130  $\mu\text{m}$  for the long and the short strips, respectively. Moreover, a threshold for the minimum deposited charge was set explicitly.

The simulation of a certain number of events produces an absolute hit count as the result. In order to extract the hit rate from this number, the simulated time must be determined from the total number of simulated events and the interaction rate which has to be provided as an input parameter. For this analysis, a constant interaction rate of  $2 \cdot 10^7 \text{ s}^{-1}$  has been assumed as it is given in the specification for the PANDA experiment [13], [14]. However, this number is only an averaged value and does not take into account experimental uncertainties. The conditions met in reality will exhibit a time-dependent profile of the interaction rate. As a consequence, count rates obtained in short time intervals will differ significantly from the averaged value. Some sources of such effects having impact on the luminosity profile are namely:

- Time dependent variations of the target density (intrinsic discontinuity), in particular in case of the pellet target.
- Change of the interaction rate during beam lifetime and beam profile due to extraction of antiprotons into the HESR.
- Change of simulated time due to momentum dependent process cross sections.

In order to deal with these uncertainties, an overall safety factor of 4 has been introduced for the final numbers allowing an estimate on the upper limits for the expected count rates in antiproton-proton collisions.

### 3.3 Simulation Results

In the following, the detailed rates for the different detector parts as well as a summary of the most active individual components are shown. In table 3 the integrated rates for all individual pixel and strip layers are summarized explicitly. Table 4 contains the maximum count rates for single channels and on frontend level within the pixel and the strip part of the MVD as well as for the additional forward strip disks.

Basically, the results obtained with *Geant 3* and *Geant 4* are in agreement with each other. However, some deviations occur as it can be seen exemplary in figure 6. The simulation using *Geant 3* yields an increased rate at higher beam momenta for the forward direction at small opening angles. This region is covered by the additional forward disks and by the inner pixel disks which are included in the MVD pixel part. Besides, a slight enhancement of the *Geant 4* data points is present for lower beam momenta at large polar angles which can be seen in the strip barrel layers only. The highest data load for individual layers appears in the strip barrel part due to the large area which is covered. However, the rates on pixel disks are already in the same order of magnitude (see figure 7). In general, the data rate for the barrel part is almost constant over the full momentum range showing even a slight decline with higher beam momenta. In contrast, the data load for the disk layer is increasing with higher beam momenta due to the prominent forward-peaked particle emission (as already discussed in figure 2).

As a consequence, the pixel part of the MVD yields the highest data load with up to 1.8 Gevts/s at maximum beam momentum. It drops to 1.2 Gevts/s for low beam

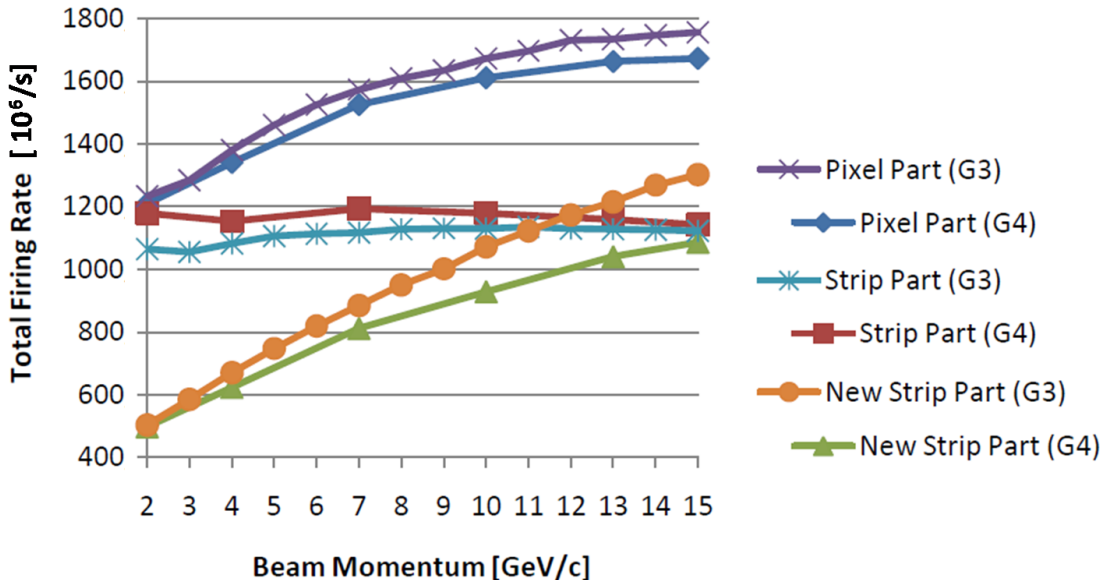


**Figure 6:** Comparison of the integrated data load for the pixel and strip part of the MVD as well as the additional forward strip disks. Results obtained with *Geant 3* (G3) and *Geant 4* (G4).

p (GeV/c)	2	4	7	10	13	15
<b>Barrel 1 Pixels</b>	149 (144)	127 (122)	106 (101)	96 (90)	86 (81)	85 (80)
<b>Barrel 2 Pixels</b>	251 (251)	230 (222)	216 (210)	208 (196)	199 (187)	195 (181)
<b>Barrel 3 Strips</b>	473 (537)	471 (512)	472 (514)	475 (508)	468 (494)	464 (485)
<b>Barrel 4 Strips</b>	390 (444)	369 (408)	358 (402)	349 (382)	339 (363)	336 (358)
<b>Disk 1 Pixels</b>	129 (122)	142 (132)	157 (148)	162 (150)	164 (153)	162 (150)
<b>Disk 2 Pixels</b>	107 (103)	133 (127)	157 (149)	167 (158)	174 (164)	174 (163)
<b>Disk 3 Pixels</b>	177 (172)	217 (214)	262 (251)	286 (274)	298 (283)	302 (292)
<b>Disk 4 Pixels</b>	155 (153)	196 (194)	246 (243)	269 (264)	289 (279)	293 (280)
<b>Disk 5 Pixels</b>	137 (140)	175 (172)	224 (220)	249 (247)	269 (263)	273 (269)
<b>Disk 6 Pixels</b>	127 (127)	159 (158)	206 (204)	236 (233)	254 (254)	262 (258)
<b>Disk 5 Strips</b>	101 (98)	123 (119)	149 (144)	158 (149)	167 (159)	169 (157)
<b>Disk 6 Strips</b>	102 (100)	120 (115)	140 (134)	149 (140)	154 (144)	154 (144)
<b>Disk 7* Inner Strips</b>	185 (179)	247 (225)	327 (298)	396 (345)	449 (386)	484 (404)
<b>Disk 7 Outer Strips</b>	91 (90)	116 (108)	142 (138)	163 (152)	174 (163)	180 (165)
<b>Disk 8* Inner Strips</b>	143 (142)	203 (190)	279 (246)	352 (288)	418 (334)	463 (359)
<b>Disk 8 Outer Strips</b>	85 (87)	105 (100)	137 (131)	160 (145)	175 (159)	180 (160)

*All values are given in Mevts/second.*

**Table 3:** Data rates (Mevts/s) for different MVD layers in antiproton-proton collisions assuming an interaction rate of  $2 \cdot 10^7 \text{ s}^{-1}$ . The values obtained with *Geant 3* are listed in the first line. For comparison, results from a complementary study using *Geant 4* and a smaller statistical sample are given in parentheses below. A safety factor of 4 is included in addition which compensates uncertainties within the experimental conditions (as explained in chapter 3.2). The results are summarized in figure 7.

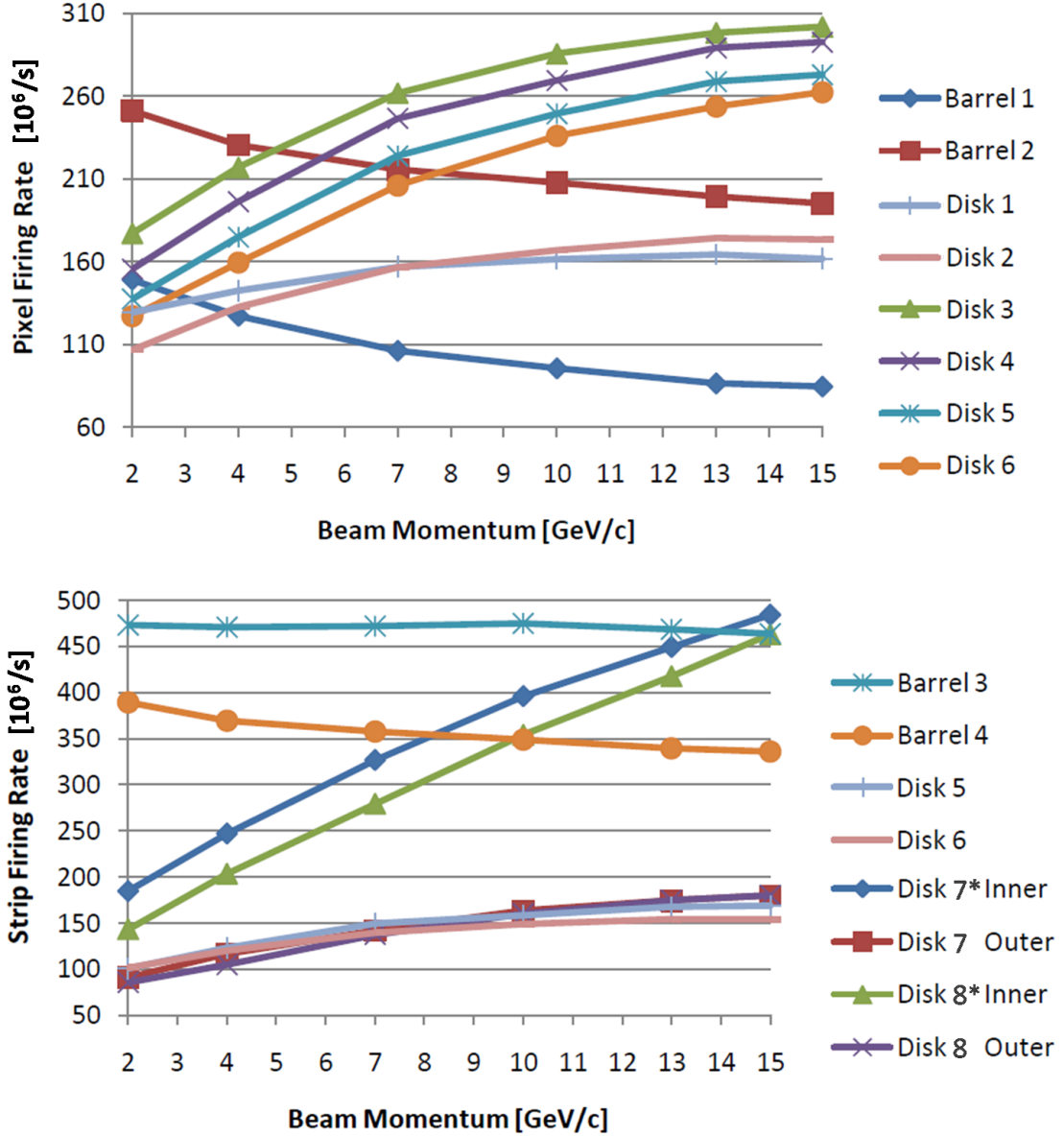


**Figure 7:** Simulated data load for different MVD layers at different initial beam momenta in DPM antiproton-proton collisions. The values are taken from table 3.

momentum. The overall data rate of the strip part stays constant over the full momentum range at a value of 1.2 Gevts/s. The hit rates within the additional forward disks are most sensitive to the beam momentum, starting at a lower data load of about 0.5 Gevts/s and reaching the same value as for the strip part at highest beam momentum. However, it should be noted that these numbers are overestimated due to the large overlap of the implemented disk structure.

The general momentum dependence as described above is again reflected by the peak rates on frontend level (see figure 8). The maximum values for the pixel and the strip frontend of the central MVD reach 9.0 Mevts/s and 2.8 Mevts/s, respectively. (see table 4). The highest rates on the strip frontend for the additional disks exceed the values obtained in the central MVD by a factor of two maximum. Finally, the maximum hit rate for single pixel cells is in the order of 10 kevts/s. For the strip frontend of the central MVD and the additional forward disks higher

p (GeV/c)	2	4	7	10	13	15
<b>Single Pixel</b>	6.4 (8.0)	6.4 (9.6)	6.4 (11.2)	6.4 (9.6)	7.2 (11.2)	6.4 (11.2)
<b>Pixel frontend</b>	6018 (6016)	7016 (7131)	7840 (7961)	8426 (8652)	8550 (9004)	8723 (9061)
<b>Single Strip</b>	29.6 (40.0)	29.6 (36.8)	31.2 (40.0)	36.0 (41.6)	33.6 (44.8)	34.4 (43.2)
<b>Strip frontend</b>	1914 (2539)	2146 (2269)	2375 (2464)	2409 (2635)	2645 (2755)	2472 (2605)
<b>Single strip (new)</b>	34.4 (40.0)	41.6 (49.6)	46.4 (56)	59.2 (65.6)	66.4 (72.0)	69.6 (73.6)
<b>Strip frontend (new)</b>	2287 (2370)	3058 (2883)	4012 (3834)	4869 (4435)	5709 (5168)	6252 (5261)

*All values are given in kevt/s/second*

**Table 4:** Peak rates (kevt/s) in antiproton-proton collisions on single channels and frontends for the MVD pixel part, the MVD strip part and the additional forward strip disks (denoted as “new”). The values obtained with *Geant 3* and *Geant 4* are listed in the first and second line, respectively. They refer to an estimated interaction rate of  $2 \cdot 10^7 \text{ s}^{-1}$  and an additional safety factor of 4 (as introduced in chapter 3.2). The results are illustrated in figure 8 and 9.

numbers of roughly 40 kevt/s and 70 kevt/s result. However, the given numbers on single channels exhibit a relatively large error due to the limited statistics. This is particularly true for single pixel cells.

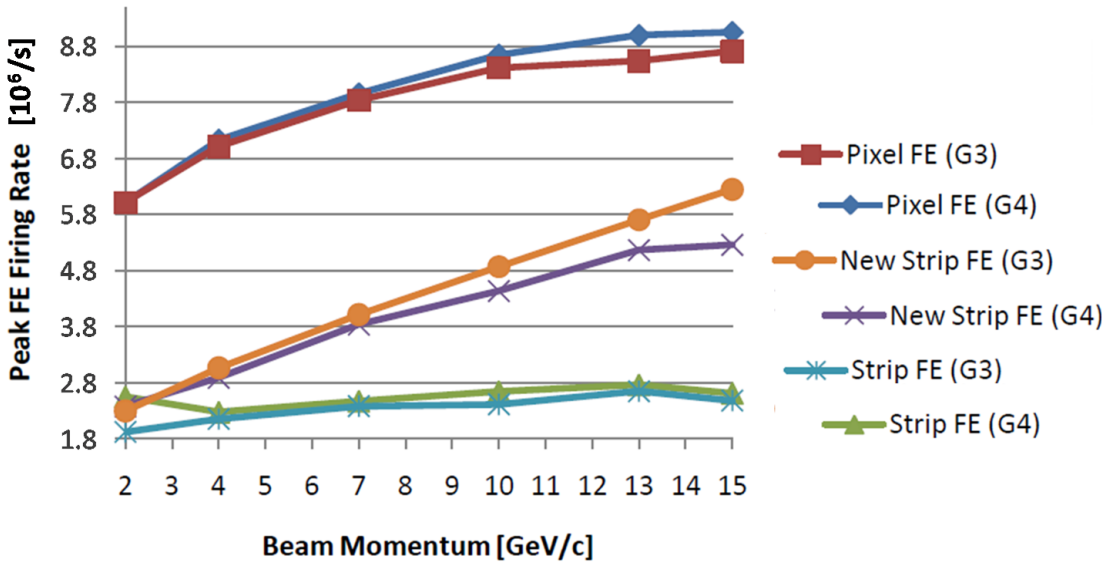


**Figure 8:** Maximum frontend rates using *Geant 3* (G3) and *Geant 4* (G4) for the MVD pixel part, the MVD strip part and the additional forward strip disks. Values are taken from table 4.

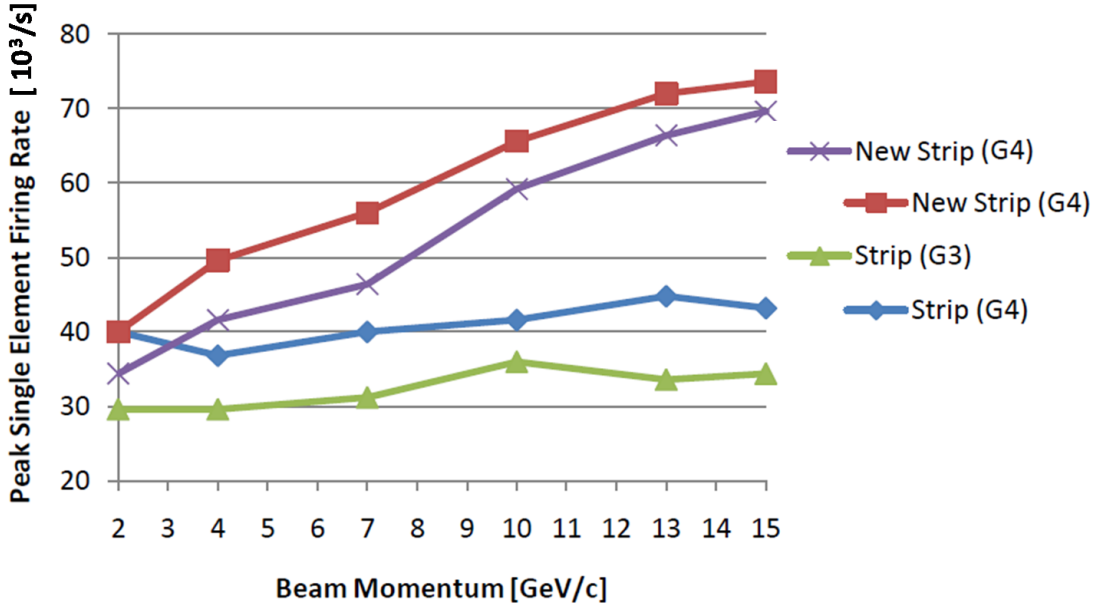


**Figure 9:** Maximum hit rates for single strips within the central MVD and the additional forward disks referring to table 4 using *Geant 3* (G3) and *Geant 4* (G4).

## 4 Summary

The count rates on single channels and frontends in different detector regions reflect the particle track distribution of all outgoing reaction particles. Peak values are obtained in the inner sectors of the forward part which cover small solid angles. However, when changing from antiproton-proton to antiproton-gold collisions, a comparable high data load will also appear in the forward barrel part. The peak rates on frontends and single channels within antiproton-nuclei reactions decrease by one order of magnitude compared to antiproton-proton reactions.

Comparing the results for antiprotons-proton collisions obtained in both complementary studies, several aspects must be considered:

- Different implemented detector models
- Dimensions of pixel cell and strip pitch
- Effective readout area for frontend chips
- Implemented safety factor

The safety factor of 4 has to be considered when comparing table 1 with table 4. Taking into account the effective readout area of the frontend chip, the maximum frontend rates extracted in the first study are higher compared to the second one: for the pixel part by 25%, in the strip part by a factor of 4 (see table 5). Mostly, the deviations can be explained by two facts:

1. No threshold setting within the digitization of the first study.
2. Geometrical effects due to the implemented detector models. The simplified model in chapter 2 delivers particularly high count rates on frontends within the inner strip disk part (see figure 4). Compared to the more realistic model used in chapter 3 this already results in a factor of more than 2.

	Antiproton-gold 1st study	Antiproton-proton 1st study	Antiproton-proton 2nd study
Interaction rate	$2 \cdot 10^5 \text{ s}^{-1}$	$2 \cdot 10^7 \text{ s}^{-1}$	$2 \cdot 10^7 \text{ s}^{-1}$
Safety factor	1	1	4
<b>Pixel part</b>			
Pixel cell size	$100 \times 100 \text{ } \mu\text{m}^2$	$100 \times 100 \text{ } \mu\text{m}^2$	$100 \times 100 \text{ } \mu\text{m}^2$
Number of pixel cells	5760 pixel	5760 pixel	10000 pixel
Readout area	$57.6 \text{ mm}^2$	$57.6 \text{ mm}^2$	$100.0 \text{ mm}^2$
Maximum count rate	0.16 Mevts/s	1.46 Mevts/s	9.06 Mevts/s
Scaling factor	6.94	6.94	1
Scaled count rate	1.1 Mevts/s	10.1 Mevts/s	9.1 Mevts/s
<b>Strip part</b>			
Strip pitch (long side)	98 / 164 $\mu\text{m}$	98 / 164 $\mu\text{m}$	120 $\mu\text{m}$
Strip length	63.0 mm	63.0 mm	66.7 mm
Readout area	790 / 1323 $\text{mm}^2$	790 / 1323 $\text{mm}^2$	1025 $\text{mm}^2$
Maximum count rate	0.10 / 0.15 Mevts/s	2.44 / 3.38 Mevts/s	2.6 Mevts/s
Scaling factor	5.2 / 3.1	5.2 / 3.1	1
Scaled count rate	0.52 / 0.47 Mevts/s	12.7 / 10.5 Mevts/s	2.6 Mevts/s

**Table 5:** Comparison of the results obtained for maximum count rates on frontend level. A scaling factor is introduced in order to compare the numbers extracted within the two different studies. It includes the additional safety factor taken into account in the second study and a geometrical factor due to the different effective readout area. However, an additional effect has to be considered due to the different implemented detector models which is not included in the scaling factor (see text). The strip modules of the first model which deliver the maximum values overestimate the count rates by more than a factor of two compared to the more realistic model implemented in the second study. The maximum count rates within antiproton-proton collisions increase by roughly one order of magnitude compared to antiproton-gold reactions.

Within the scope of a more dedicated estimate of upper limits for maximum frontends rates, numbers converge at roughly 10 Mevts/s for the pixel and 5 Mevts/s for the strip part. The overall data load of the MVD adds up to a maximum value of roughly 3 Gevts/s. The overall data load for the MVD in antiproton-gold collisions is lower than for antiproton-proton collisions.

## 5 Outlook

Obviously, the extraction or estimate of maximum count rates and overall detector data load depends on four main input parameters:

- Implemented detector model
- Simulation software

- Assumed interaction rate
- Safety factor

Hence, the numbers must be further surveyed during ongoing detector development. Since the mechanical design is already in an advanced stage and the basic layout is frozen, changes due to modification within the detector layout are expected to be rather small. The last significant revision of the detector layout compared to the one used in chapter 3 was due to the increased opening angle of the beam pipe in upstream direction and resulted in a reduced number of sensors in the strip barrel layers. Besides the overall data load of the MVD strip part, which is even lowered, it has no impact on the maximum frontend rates therein.

The main modification on the simulation software may be on the implementation of the Coulomb part to the elastic scattering. However, this particular effect is only relevant in the region around  $90^\circ$  since the second elastic peak does not affect the MVD. As a consequence, maximum frontend rates within the barrel part probably increase by some fraction. In this case it must be checked if they exceed the maximum values obtained in the forward disks. Furthermore, a dedicated study with antiproton-nucleon reactions complementary to the one in chapter 2 is strongly desirable.

The most delicate item is the initial interaction rate to be assumed for the experiment which has an enormous impact on the final numbers. Therefore, a proper description of the beam-target interaction is necessary for both antiproton-proton and antiproton-nucleon reactions. As discussed in chapter 3.2, this includes a precise definition of the beam conditions as well as a clear evaluation of the target quality in order to obtain reliable numbers for both the average and the peak luminosity. While the average luminosity is a result of an integration over a sufficiently long time (at least several duty cycles), the peak luminosity refers to a short time constant which is connected to the defined clock standard for the PANDA experiment. The clock frequency is not fixed yet but in the order of 50 MHz up to 125 MHz. Hence, the time resolution needed for a precise description of the beam-target interaction must be better than 10 ns.

In the current status, a lot of the issues discussed above are still missing or undefined. Therefore, all uncertainties have to be summed into one quite conservative safety factor. The chosen safety factor must be reasonable to prevent an unnecessary overestimation. Certainly, better specifications of the experimental conditions within PANDA are crucial for optimization and further ASIC development. New studies on the MVD count rates and the data load become meaningful only with an improved input and reliable numbers given for the beam-target interaction.

## References

- [1] PANDA wiki: MVD web, Developer's area  
<http://panda-wiki.gsi.de/cgi-bin/view/Mvd/FEspecs> <sup>1</sup>  
*Specifiaction list: Pixel frontend (a) and Strip frontend(b)*  
 (a) [http://panda-wiki.gsi.de/pub/Mvd/FEspecs/Parameter\\_list\\_020409.doc](http://panda-wiki.gsi.de/pub/Mvd/FEspecs/Parameter_list_020409.doc)  
 (b) [http://panda-wiki.gsi.de/pub/Mvd/FEspecs/fe\\_specs.pdf](http://panda-wiki.gsi.de/pub/Mvd/FEspecs/fe_specs.pdf)
- [2] A. Capella, U. Sukhatme, I. Tanc, J. Tran Thanh Vana: *Dual parton model*;  
 Phys. Rept. **236** (1994) 225-329
- [3] A. Galoyan, J. Ritman, A. Sokolov, V. Uzhinsky: *Parametrization of the  $\bar{P}P$  Elastic Scattering Differential Cross Section Between  $2\text{ GeV}/c \leq P_{lab} \leq 16\text{ GeV}/c$* ; arXiv:0809.3804v1 [hep-ex]; 2008
- [4] M. Bleicher et al: *Relativistic hadron-hadron collisions in the ultra-relativistic quantum molecular dynamics model*; J. Phys. G: Nucl. Part. Phys. **25** (1999) 1859-1896
- [5] S. A. Bass et al: *Microscopic Models for Ultrarelativistic Heavy Ion Collisions*  
 Part. Nucl. Phys. **41** (1998) 255-369
- [6] R. Jäkel: *Resolution Studies for the Micro Vertex Detector of the PANDA Experiment and the Reconstruction of Charmed Mesons for Specific Hadronic Channels*; PhD thesis, Technische Universität Dresden, 2009
- [7] BaBar collaboration: *Workbook for BaBar users - online documentation*.  
<http://www.slac.stanford.edu/BFROOT/www/doc/workbook/workbook.html>
- [8] *GEANT Detector Description and Simulation Tool*; CERN Program Library  
 Writeup W5013, 1993
- [9] S. Agostinelli et al: *Geant 4 — a simulation toolkit* ; Nucl. Instrum. Meth. **A 506**  
 (2003) 250-303
- [10] J. Alliso et al: *Geant 4 Developments and Applications*; IEEE Trans. Nucl. Sci. **53**  
**No.1** (2006) 270-278
- [11] S. Spataro *Simulation and event reconstruction inside the PandaRoot framework* J.  
 Phys. Conf. Ser. **119** (2008) 032035
- [12] PANDA wiki: MVD web, Developer's area  
*Documentation:* <http://panda-wiki.gsi.de/cgi-bin/view/Mvd/ModelMvd1pt0><sup>1</sup>  
*Technical Drawings: Pixel part (a) and Strip part(b)*  
 (a) [http://panda-wiki.gsi.de/pub/Mvd/ModelMvd1pt0/Pv-1.0\\_Documentation.pdf](http://panda-wiki.gsi.de/pub/Mvd/ModelMvd1pt0/Pv-1.0_Documentation.pdf)  
 (b) [http://panda-wiki.gsi.de/pub/Mvd/ModelMvd1pt0/Sv-1.0\\_Documentation.pdf](http://panda-wiki.gsi.de/pub/Mvd/ModelMvd1pt0/Sv-1.0_Documentation.pdf)
- [13] PANDA collaboration: *PANDA - Strong Interaction Studies with Antiprotons, Technical Progress Report*; 2005
- [14] PANDA Collaboration: *Physics Performance Report for: PANDA - Strong Interaction Studies with Antiprotons*; arXiv:0903.3905v1; 2009

---

<sup>1</sup>Restricted area, in case of denied access use contacts given on public pages to obtain the relevant information